

Article

Numerical Simulation of the Influence of Hydrogen Concentration on Detonation Diffraction Mechanism

Mohammad Hosein Shamsadin Saeid ¹  and Maryam Ghodrat ^{2,*} ¹ Department of Mechanical Engineering, University of Birjand, Birjand 97175615, Iran² School of Engineering and Information Technology, University of New South Wales Canberra, Canberra, ACT 2610, Australia

* Correspondence: m.ghodrat@unsw.edu.au

Abstract: In this study, the impact of hydrogen concentration on deflagration to detonation transition (DDT) and detonation diffraction mechanisms was investigated. The combustion chamber was an ENACCEF facility, with nine obstacles at a blockage ratio of 0.63 and three mixtures with hydrogen concentrations of 13%, 20%, and 30%. Detonation diffraction mechanisms were numerically investigated by a density-based solver of OpenFOAM CFD toolbox named ddtFoam. In this simulation, for the low Mach numbers, the pddtFoam solver was applied, and for high speeds, the pddtFoam solver switched to the ddtFoam solver to simulate flame propagation without resolving all microscopic details in the flow in the CFD grid, and to provide a basis for simulating flame acceleration (FA) and the onset of detonation in large three-dimensional geometries. The results showed that, for the lean H₂–air mixture with 13% hydrogen concentration, intense interaction between propagating flame and turbulent flow led to a rapid transition from slow to fast deflagration. However, the onset of detonation did not occur inside the tube. For the H₂–air mixture with 20% hydrogen concentration, the detonation initiation appeared in the acceleration tube. It was also found that following the diffraction of detonation, the collision of transverse waves with the wall of the tube and the reflection of transverse waves were the most essential and effective parameters in the re-initiation of the detonation. For the H₂–air mixture with 30% hydrogen concentration, the detonation initiation occurred while passing through the obstacles. Subsequently, at detonation diffraction, the direct initiation mechanism was observed.

Keywords: CFD; heat and mass transfer; detonation diffraction; ddtFoam

Citation: Shamsadin Saeid, M.H.; Ghodrat, M. Numerical Simulation of the Influence of Hydrogen Concentration on Detonation Diffraction Mechanism. *Energies* **2022**, *15*, 8726. <https://doi.org/10.3390/en15228726>

Academic Editor: Adonios Karpetis

Received: 10 October 2022

Accepted: 14 November 2022

Published: 20 November 2022

Publisher's Note: MDPI stays neutral with regard to jurisdictional claims in published maps and institutional affiliations.



Copyright: © 2022 by the authors. Licensee MDPI, Basel, Switzerland. This article is an open access article distributed under the terms and conditions of the Creative Commons Attribution (CC BY) license (<https://creativecommons.org/licenses/by/4.0/>).

1. Introduction

Hydrogen is being introduced as a zero-emission energy carrier in the road transport sector. Hydrogen cars are expected to play an essential role in a clean-transport future. Accidental hydrogen release in an open-air environment will disperse quickly, not causing significant hydrogen hazards. A hydrogen hazard is more likely to occur when hydrogen is accidentally released in a confined place such as a road tunnel. Hydrogen cars in a tunnel would no doubt lead to more concerns about the safety of the tunnel. Due to the low ceiling height and confined space, a fire in a tunnel has always had more serious consequences than a fire in the open air. The main problem in transport is the safe use of hydrogen in road tunnels where hydrogen release could end in fire, deflagration, and even detonation [1]. The two combustion modes of deflagration and detonation are generally distinguished from each other. A deflagration occurs when a flame front travels by transferring heat and mass to the unburned mixture ahead of the front. The deflagration wave propagates at subsonic speed. However, a detonation wave is a supersonic compression shock wave that ignites the mixture by adiabatic heating across the leading shock front. Over the years, various phenomena in detonation have been studied. Detonation transition from one channel to a larger one or a fully open environment, one of the essential applications of detonation

in propulsion systems, is known as detonation diffraction and has wide applications in the military, detonation engines, and the safety of transporting explosive materials [2]. Detonation diffraction occurs in either sub-critical, critical, or supercritical regimes and depends on the composition of the mixture, initial thermodynamic conditions, and the system geometry [3–5]. In a sub-critical regime, the sudden expansion of the channel causes cooling of the detonation surface by the expansion waves, inducing the separation of the reaction zone and the precursor shock wave. Consequently, the sub-critical regime is the one in which a complete failure of the detonation wave occurs. The energy release rate dominates the expansion rate in the supercritical regime, maintaining the coupling between the shock and reaction zone, which permits a successful transition across the area change. The critical state demonstrates the initial state of the gas mixture separating the sub-critical and supercritical regimes. In a specific criterion for the critical regime in fuel–air and undiluted fuel–oxygen mixtures, the diameter of tube d must be 13 times larger than the detonation cell λ [6–8].

Detonation propagation in obstacle channels and channels with an absorbent wall was carried out in the works of Teodorczyk et al. [9] and Dupre et al. [10]. The findings of these studies proved the essential role of transverse waves in detonation propagation. These authors also found that transverse waves can be the source of the mechanism that renders the intense combustion of the detonation mode. Similarly, detonation phenomena such as the detonation initiation, transition of the detonation expansion from a channel or tube to an open environment, and collapse of the detonation wave were investigated by Lee [11], Knystautas et al. [6], and Moen et al. [7]. These authors found that there are two detonation initiation modes: a slow detonation mode that is formed with an accelerating flame, and a fast detonation mode that is generated “instantaneously” when an adequately strong igniter is used. Li et al. [12] investigated different types of alternative fuel vehicles and carried out an analysis of the peak overpressure in case of an explosion in a tunnel. Their results showed that, for hydrogen vehicles, the fire sizes were significantly higher compared to CNG tanks, while flame lengths were only slightly longer. Furthermore, for gas cloud explosions, the maximum overpressure was mostly found somewhat further than the end of the gas cloud. There was generally a growth tendency before the position, with maximum overpressure due to the increasing flame speed, and a decay tendency after it. In the far field, the overpressure decayed along the distance much more slowly. In some cases, deflagration to detonation occurred.

In most research on the acceleration of flame and DDT inside obstructed channels, the obstacle results in flame acceleration and increased explosion overpressure in a closed chamber or channel. Gamezo et al. [13] numerically investigated FA and DDT in obstructed channels. Their results showed that the thermal expansion of hot combustion products caused flame acceleration at the initial stages. After that, shock–flame interactions, RM, RT, and KH instabilities, and flame–vortex interactions in obstacle wakes became responsible for the increase in the energy release rate, the flame surface area, and the shock strength. When the leading shock became strong enough, detonations emerged from hot spots generated by shock reflections at corners between the wall and obstacles. Furthermore, they concluded that by placing obstacles in semi-closed channels, the flame surface area and the amount of turbulence produced would increase, while the distance to DDT declined. Ciccarelli et al. [14] presented a review of FA and DDT in obstructed and unobstructed ducts. The laminar flame that results from the weak ignition of a combustible mixture is classified as an inherently unstable combustion phenomenon. The interactions of flame with obstacles and confinement, as well as its instabilities, increase its surface area and burning rate. Finally, the flame becomes turbulent and accelerates through a series of turbulent combustion regimes. This process, known as flame acceleration, may create a hot spot in the flame propagation under certain initial and boundary conditions that may lead to the onset of detonation. The DDT in obstructed channels was examined numerically by Kessler et al. [15] and Na’Inna et al. [16]. Their findings showed that placing obstacles leads to a reduction in the distance to DDT and an increase in the flame surface area in

semi-closed channels. Hydrogen has been organized in the framework of the SARNET network by Bentaib et al. [17]. They believed that turbulence impact on flame deceleration, flame acceleration, and flame quenching mechanisms was not well reproduced by the combustion models usually implemented in safety tools, and further model enhancement and validation were needed. For this aim, three tests were performed in the ENACCEF facility. They examined vertical flame propagation in a homogenous mixture with 13% hydrogen concentration and blockage ratios of 0, 0.33, and 0.6. Their results presented the benchmark conclusions regarding the ability of CFD combustion models to predict the impact of turbulence on flame propagation. Emami et al. [18] numerically studied the process of DDT in an obstructed channel with a stoichiometric H₂-air mixture. They used a 2D simulation of large vortices and an artificially thickened flame approach to simulate sub-grid combustion modeling. Their results showed that the flame-eddy interaction and flame wrinkling were the main mechanisms in escalating the flame surface area and flame propagation in deflagration regimes. In their numerical simulations, they showed that the primary mechanism of flame propagation at high velocities is the interaction of reflected shocks and vortices formed because of the baroclinic mechanism. Hasslberger et al. [19] used the OpenFOAM version 2.1.x to simulate a RUT facility at a hydrogen concentration near the lower deniability limit. The code was written in C++, and adaptive mesh refinement (AMR) was used to reduce computational costs. The RUT facility had three parts: an obstructed channel, a canyon, and a curved channel. The numerical flame acceleration results were compared with two experiments. The first simulation, with a hydrogen concentration of 14%, was well predicted for the distance of the DDT at the reflecting surface. The second simulation, with a hydrogen concentration of 12.5%, did not observe a successful transition. Nevertheless, in the experiment for the hydrogen concentration of 12.5%, the onset of detonation was reported. Cicarelli et al. [20] experimentally examined the detonation propagation mechanism in a tube with orifice plates. Their results showed that, for orifice plates that were below the critical tube diameter, detonation propagation occurred because of re-initiation on the tube wall at hot spots. At the detonation propagation limit (critical orifice diameter), detonation propagation relied on a single hot spot to form. Furthermore, for larger orifice plate spacing, many hot spots formed downstream of the orifice plate and the resulting detonation waves merged before the next orifice plate. Zhu et al. [21] investigated flame acceleration and DDT in a mixture of NH₃-H₂-O₂ in obstructed channels. Their simulations showed that in the mixture of NH₃-O₂ without H₂, the flame could not propagate. Nevertheless, when the hydrogen concentration without ammonia surged to 100%, an explosion center emerged, and detonation was initiated. Ni et al. [22] studied the DDT process in the hydrogen mixture and investigated the impact of the blockage ratio of arc obstacles using OpenFOAM. They used the HLLC scheme to determine convective fluxes. This scheme was suitable for shock capturing. They found that by increasing the blockage ratio, the flame velocity would be higher, and the DDT run-up distance was decreased by arc obstacles. As reported by their research, the most efficient blockage ratio for curved obstacles is 0.7. Sun et al. [23] experimentally examined the impact of the orifice plate and hydrogen mole fraction on different regimes of the onset of detonation. Their results showed that the regimes of fast flame and steady detonation were observed in the smooth duct. By placing a square orifice plate in the duct, three different regimes of the onset of detonation were observed. i) For the low limit, the passage of the flame through the orifice plate caused detonation decay and detonation re-ignition did not occur. ii) Increasing the hydrogen mole fraction caused the detonation wave to be re-initiated after the detonation decay. iii) For the high hydrogen concentration limit, the fast flame was produced, and a stable detonation wave was not observed. Shamsadin Saeid et al. [24] investigated the detonation initiation mechanisms in an inhomogeneous and a homogeneous mixture of H₂-air inside a combustion chamber with BR = 0.3. The results showed that, in the homogeneous mixture of H₂-air at a concentration of 30%, with changes in the obstacles' spacing-to-height ratio, two different scenarios could be observed. At an obstacles' spacing-to-height ratio greater than three (S/H > 3), the shock

collision ahead of the flame and the shock–flame interaction provided the conditions for detonation initiation. At an obstacles' spacing-to-height ratio less than or equal to three, flame jets through the obstacles led the pressure to be concentrated at the front of the flame, where an explosion center was noticed at the leading edge, and the DDT occurred owing to converging shock waves. Liu et al. [25] used OpenFOAM to simulate FA and DDT in different obstructed channels with inhomogeneous mixtures. They combined the HLLC Riemann solver and the PISO solver, and their results revealed that the new solver had less numerical dissipation at the discontinuity point as well as the ability to predict the flame speed and shockwave position. They also analyzed the changes in density, pressure, and the flame front with time, and showed that the onset of detonation is led by the interaction between the front shock wave and obstacles and the duct walls. The entire DDT process begins from a local explosion and continues until the flame front achieves the front shock wave to construct a stable explosion combustion surface. Soleimanpour et al. [26] used OpenFOAM to examine the DDT of H_2-O_2 in two-dimensional porous closed channels. They coupled a density-based hybrid solver and pressure-based solver with Godunov-type schemes. Their results indicated that changes in the blockage ratio of obstacles and the interval between obstacles led to considerable variations in DDT structure. Moreover, using porous obstacles and the porous zone is an advanced method for controlling the DDT process.

In recent decades, various analytical, numerical, and experimental studies have investigated detonation diffraction [27,28]. Schultz [29] presented an analytical relationship for calculating critical diameters. He wrote that evaluation of the critical tube diameter requires knowledge of seven parameters: specific heat ratio, CJ detonation velocity, critical shock velocity, post-shock reaction time, effective activation energy parameter, disturbance propagation angle, and acoustic speed. Although the results of his analytical model were somewhat consistent with some experimental results, in some detonations, especially those with irregular cell structures, the analytical and experimental results differed significantly. Papalexandris et al. [30] numerically studied the behavior of 2D detonation waves propagating from a small duct to a larger chamber. They parametrically inspected the impacts of the gas mixture activation energy and the cross-sectional channel ratio on the regime governing the detonation diffraction. They used symmetrical geometry to simulate the detonation diffraction in the channel. Their results showed that sufficiently large values of these two parameters can lead to critical or sub-critical regimes. They further examined the diffraction of the over-driven detonation instead of the CJ detonation, and performed three-dimensional simulations of detonation diffraction. They concluded that the regime governing the detonation diffraction in 3D was similar to that in 2D. Sun et al. [31] experimentally studied the influence of an orifice plate on the regimes of detonation transmission in a cylindrical tube. They observed the sub-critical condition and the super-critical condition in an unobstructed tube. However, in the tube with a single orifice plate, the critical condition was observed for detonation re-initiation. Zheng et al. [32] experimentally investigated different modes of detonation initiation in combustion chambers with pre-detonator tubes. The results revealed that, based on the composition of the mixture and the tube length, four types of reaction waves were produced and used to initiate detonation in the main chamber: the deflagration ignition wave, high-speed deflagration ignition wave, CJ detonation ignition wave, and the over-driven detonation ignition wave. Four mechanisms to initiate detonation, i.e., direct initiation, slow and fast deflagration to detonation transition initiation, and local explosion initiation, were observed in the main chamber. Lei et al. [33] experimentally investigated the influence of various lengths of pre-detonators and a variety of mixtures in initiating detonation in the downstream chamber. They showed that the successful transition of detonation waves can occur into the main chamber when the pre-detonator critical diameter (d_c) experiences a greater size than the cell of detonation (λ). For different fuel–air mixtures, the critical transmission ratio ($k_c = d_c/\lambda$) is 13. As reported by their research, the successful transition of the detonation wave could be mainly categorized into three methods. The first one is to reduce λ by including more reactive

mixtures into the pre-detonator. The second method utilizes barriers (such as the reflecting board, the backward-facing step, or any other configuring items). The third one is to use an overdriven detonation.

A detailed survey of the existing literature revealed that most of the work carried out on detonation has been based on experimental results [34–38] and required staggering expenditures. As detonation is a high-speed phenomenon of microsecond order, observing many of the properties of detonation with experimental methods needs advanced and expensive techniques and is sometimes impossible. Therefore, it is necessary to use numerical simulation, which is a powerful and appropriate instrument. As mentioned above, numerical examinations of the behavior of the detonation during diffraction are needed. Hence, using numerical simulation, the current study explored the transition of detonation from a small to a large tube in an ENACCEF facility [17]. The impact of different hydrogen concentrations on FA and DDT occurrence inside the tube, as well as their effects on detonation regimes during diffraction and the mechanisms governing the reinitiating of detonation, were also investigated.

In this study, mixtures with hydrogen concentrations of 13%, 20%, and 30% were used to investigate how different hydrogen concentrations alter flame propagation, and the successful transition of a pre-detonator to a larger chamber for practical air-breathing detonation engines. In general, when the hydrogen concentration in the mixture is less than 18%, the transition to detonation does not occur. Previous experimental [17] and numerical [38–42] studies in the ENACCEF facility shed light on the slow-to-fast deflagration involved with a hydrogen concentration of 13%. In this study, however, mixtures with hydrogen concentrations of 13%, 20%, and 30% were investigated. In the experiment [17], the mixture was ignited using two thin tungsten electrodes with a high-voltage source. The estimated igniter energy was about 10–20 mJ. In this simulation, a simple ignition model is used. The spark is modeled by a hot semi-circular region with a reaction progress variable of 1. Due to the ignition phase needing the solution of Navier–Stokes equations with detailed chemistry, the first short ignition phase is not modeled. The spark radius of 10 mm is utilized and any small changes in the spark radius cause some time shift of the results [16], with no effect on the physics of combustion.

Detonation diffraction conditions, from small pre-detonator tubes to main combustor tubes, are necessary for applications such as detonation engines, aerospace propulsion, and military and nuclear power stations. Moreover, the mechanism of re-initiation or failure is important from a fundamental viewpoint. Very few simulations of the mechanism of detonation diffraction in a hydrogen–air mixture are available. Herein, efforts were made to numerically examine the impact of hydrogen concentration on deflagration to detonation, and the underlying mechanisms responsible for detonation diffraction and re-initiation. The current numerical simulation results contribute to a better comprehension of fundamental physical processes on the propagation, initiation, and diffraction of the detonation phenomenon, and, therefore, help in advancing the wealth of knowledge in safety measures for industry-scale accidents to determine and control the possibility of explosion in the accidental release of hydrogen into the air due to high-pressure pulses and shock waves, which can damage industrial facilities seriously. The investigation of such phenomena requires validated codes with a high level of accuracy. Another key outcome of the present study is the recognition of similarities and differences underlying the detonation diffraction mechanism, numerically compared to recent experimental results.

2. Numerical Modeling and Governing Equations

2.1. Characteristics of ENACCEF Facility

In the present study, the ENACCEF facility situated in Orleans, France was studied [17]. The vertical vessel was 5 m in length and consisted of two parts: an acceleration tube with 0.154 m inner diameter and 3.3 m length, and a dome region with 0.738 inner diameter and 1.7 m length. There were nine annular obstacles in the acceleration tube, creating a blockage ratio of 63%. The blockage ratio is defined as $BR = 1 - (d/D)^2$, in which D and d are the

inner diameters of the acceleration tube and obstacle, respectively. The first obstacle was set 0.776 m from the tube, and expected to play an essential role in a clean-transport future bottom (point (0,0)), as shown in Figure 1. The distance between each subsequent obstacle was 0.154 m, and their width was 2 mm. The full schematic of the ENACCEF facility is illustrated in Figure 1. This combustion chamber was used to investigate the impact of hydrogen concentration in a hydrogen–air mixture on DDT and detonation diffraction mechanisms. Three hydrogen concentrations of 13%, 20%, and 30% were used to run the simulations.

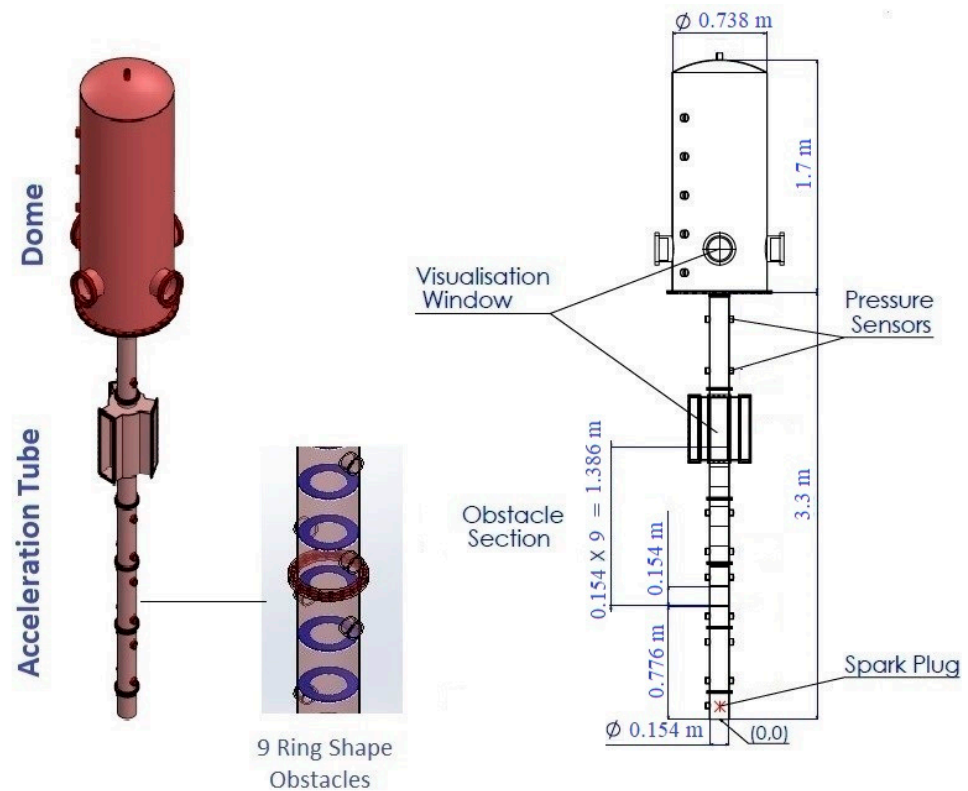


Figure 1. The schematic of the combustion chamber [17].

The initial conditions were selected according to the experiment. Because few tests have been conducted in high initial conditions, standard ambient initial conditions were determined at the ENACCEF facility. Heat loss to the walls was considered negligible for the fast explosion processes studied. The no-slip and adiabatic boundary conditions have been used for borders. The facility was not vented during the experiment; thus, a closed system was modeled, and the inlet and outlet boundary conditions were a no-slip wall. In numerical studies, exactly identical initial and boundary conditions cannot be assured in experiments of the same type.

2.2. Governing Equations

In recent years, flame acceleration and DDT have been examined in many studies using the Unsteady Reynolds-Averaged Navier–Stokes (URANS) method [43–47]. These studies have reported a URANS capability of reconstructing flame behavior interacting with obstacles, as well as the transient phenomena occurring in the DDT. The URANS method is widely used in industrial simulations because it is cost-effective and less computationally demanding compared to the Large Eddy Simulation (LES) and the Direct Numerical Simulation (DNS) methods. In the present study, the URANS method was used to model turbulent flow, and the focus of this research was, therefore, placed on fundamental detonation phenomena and behavior of detonation propagation rather than the micro-

structure of detonation. Therefore, small-scale mechanisms were not necessarily solved for this aim.

For the current premixed compressible combustion flow, the conservation of mass, momentum, energy, and reaction progression variables were solved. These time-averaged equations can be written as:

$$\frac{\partial \bar{p}}{\partial t} + \frac{\partial}{\partial x_j} (\bar{\rho} \tilde{u}_j) = 0, \tag{1}$$

$$\frac{\partial}{\partial t} (\bar{\rho} \tilde{u}_i) + \frac{\partial}{\partial x_j} \left(\bar{\rho} \tilde{u}_i \tilde{u}_j + \frac{2}{3} \delta_{ij} \bar{\rho} k \right) = -\frac{\partial \bar{p}}{\partial x_i} + \frac{\partial}{\partial x_j} \left((\mu + \mu_T) \left(\frac{\partial \tilde{u}_i}{\partial x_j} + \frac{\partial \tilde{u}_j}{\partial x_i} - \frac{2}{3} \delta_{ij} \frac{\partial \tilde{u}_m}{\partial x_m} \right) \right) + \bar{\rho} g_i, \tag{2}$$

$$\frac{\partial}{\partial t} (\bar{\rho} \tilde{e}_t) + \frac{\partial}{\partial x_j} ((\bar{\rho} \tilde{e}_t + \bar{p}) \tilde{u}_j) = \frac{\partial}{\partial x_j} \left(\bar{\rho} (a + a_T) \frac{\partial (\tilde{e}_t + \frac{\bar{p}}{\bar{\rho}})}{\partial x_j} + \mu \left(\frac{\partial \tilde{u}_i}{\partial x_j} + \frac{\partial \tilde{u}_j}{\partial x_i} - \frac{2}{3} \delta_{ij} \frac{\partial \tilde{u}_m}{\partial x_m} \right) \tilde{u}_i \right), \tag{3}$$

$$\frac{\partial}{\partial t} (\bar{\rho} \tilde{c}) + \frac{\partial}{\partial x_j} (\bar{\rho} \tilde{u}_j \tilde{c}) = \frac{\partial}{\partial x_j} \left(\bar{\rho} (D + D_T) \frac{\partial \tilde{c}}{\partial x_j} \right) + \bar{\omega}_{c,def} + \bar{\omega}_{c,ign}, \tag{4}$$

where the terms $\rho, u, p, \mu_T, \delta_{ij}, g, e, a_T, c, D_T, \omega_{c,def}, \omega_{c,ign}$ are density, velocity, pressure, turbulent flow viscosity, Kronecker delta, body forces, internal energy, turbulent thermal conductivity, reaction progress variable, turbulent molecular diffusion coefficient, Deflagrative source term, and Ignition source term, respectively. Equation (4) is solved numerically. The values of each reaction component are pre-calculated and tabulated, and the results are selected according to the results of $\tilde{c}(x, t)$ in the simulation process. The RANS version of the Weller combustion model [48] with factors $0 \leq G \leq 1$ was used for the deflagration source term. Quenching turbulent flames was considered using the following equation:

$$\bar{\omega}_{c,def} = \bar{\rho} S_T |\nabla \tilde{c}| G \tag{5}$$

$$S_T = \zeta S_L \tag{6}$$

where ρ represents the density of the unburned mixture and S_T represents the turbulent burning speed, which is modulated by the laminar burning speed S_L and the flame wrinkling factor ζ . The relationship between the laminar burning speed, temperature, and pressure is as follows:

$$S_L = S_{L,0} \left(\frac{T}{T_0} \right)^\alpha \left(\frac{P}{P_0} \right)^\beta \tag{7}$$

where α and β are 1.7 and -0.2 , respectively.

The ideal gas equation of state ($p = \rho RT$) relates pressure, density, and temperature to each other, in which R represents the specific gas constant of the mixture and T is temperature.

2.3. Turbulence Model

The role of turbulence in simulating the DDT is essential. The turbulence model applied in this simulation was the two-equation model of SST $k-\omega$. This turbulence model based on RANS can be written as:

$$\frac{\partial}{\partial t} (\bar{\rho} k) + \frac{\partial}{\partial x_i} (\bar{\rho} k \tilde{u}_i) = \frac{\partial}{\partial x_j} \left(\left(\mu + \frac{\mu_T}{\sigma_k} \right) \frac{\partial k}{\partial x_j} \right) + 2\mu_T S_{ij} S_{ij} - \frac{2}{3} \bar{\rho} k \frac{\partial \tilde{u}_i}{\partial x_i} \delta_{ij} \tag{8}$$

$$\frac{\partial}{\partial t} (\bar{\rho} \omega) + \frac{\partial}{\partial x_i} (\bar{\rho} \omega \tilde{u}_i) = \frac{\partial}{\partial x_i} \left(\left(\mu + \frac{\mu_T}{\sigma_{\omega,1}} \right) \frac{\partial \omega}{\partial x_i} \right) + \gamma_2 \left(2\bar{\rho} S_{ij} S_{ij} - \frac{2}{3} \bar{\rho} \omega \frac{\partial \tilde{u}_i}{\partial x_i} \delta_{ij} \right) - \beta_2 \bar{\rho} \omega^2 + 2 \frac{\bar{\rho}}{\sigma_{\omega,2} \omega} \frac{\partial k}{\partial x_j} \frac{\partial \omega}{\partial k} \tag{9}$$

In the above equations, the turbulent kinetic energy $k = \frac{1}{2} \tilde{u}_i \tilde{u}_j$, specific turbulent dissipation rate $\omega = \frac{\epsilon}{k} \beta^*$, and model coefficients $\gamma_2 = 0.44, \beta_2 = 0.083$, and $\beta^* = 0.09$ [25,49].

2.4. Combustion Model

In the present work, the chemical reaction rate was modeled using the flame surface wrinkling (FSW) combustion model first introduced by Weller et al. [48] as an alternative to flame surface density (FSD) models. In this model, the flame is considered as a wrinkled surface, separating burned and unburned materials. In premixed systems, combustion occurs as a thin flame, and if the flame surface area moves, the conversion of the unburned mixture to burned products will begin. Therefore, the premixed configured combustion model separates the combustion flow field into unburned and burned areas. These two areas are divided by the flame [50].

Herein, to obtain the most proper form of the equations and based on Navier–Stokes reaction equations, several assumptions were considered. The 2D modeling was applied as the first simplifying assumption. The onset of detonation has a complex 3D structure, and to achieve the most realistic response, all equations had to be expanded in 3D. Across various experimental studies in this field, to change the 3D problem to a 2D state, the DDT process in ducts with low height and long length has been studied. Gamezo et al. [13] examined the detonation phenomenon numerically in ducts. Their simulations indicated that the flame becomes more wrinkled in the 3D state; nevertheless, flame development is dominated by RM instability. Therefore, numerical studies of 3D and 2D problems illustrate the same results. Another assumption was the use of the complete gas state equation for reactants and combustion products. The temperature and pressure range of the deflagration and denotation are such that the assumption of an ideal gas was considered as a reasonable presumption [51].

2.5. Numerical Method

In general, many numerical studies have explored the underlying physical mechanisms of FA and DDT. The developed methods are based on entirely resolved reactive Navier–Stokes equations accompanied by details of reaction kinetics. Our understanding of the microscopic interactions between the turbulence, instabilities, and shock–flame interactions that are involved in DDT are enhanced by such modeling efforts. Whenever these models can depict the physics of a problem in complete detail, they are partly restricted to simple and small domains because of the necessity of a considerable number of grids. In the field of hydrogen safety, for complete control over industry-scale accidents, enlarging the scale of highly resolved simulations increases the computational need to a limit beyond the present resources and capabilities. As a result, an alternative modeling method is needed to calculate flame propagation properties and pressure transients without compromising accuracy in large geometries in an acceptable computational time. Significant progress has also been made in this area [19,44,52]. Hasslberger et al. [19] used the OpenFOAM package to simulate an RUT facility with a grid size of 7 cm to reduce computational costs. They used under-resolve meshes in order to be applicable when simulating large-scale scenarios.

In the current numerical simulation, the main purpose of the present work was to calculate macroscopic shock propagation properties and flame characteristics. A coarse grid size was used in the simulation; under-resolved grids prepare computational scalability for greater areas and allow flame acceleration and DDT studies in a time-limited manner. In the present study, the RANS modeling approach was selected because it is computationally cost-effective, and a large mesh size can be partly used. In addition, RANS modeling provides a relatively good estimation of the macroscopic parameters. The PISO algorithm and ddtFoam solver [43,53] were combined to simulate flame propagation and to provide a basis for simulating FA and DDT in large geometries. The PISO algorithm, using the flame wrinkling combustion model, has been developed and named as pddtFoam (which is based on the available XiFoam solver in OpenFOAM). The pddtFoam solver is suitable for Mach numbers less than 0.3, while the ddtFoam solver with the value of Mach numbers more than 0.3 is activated to predict the place of DDT occurrence. In the initial stage of flame propagation, a pressure-based solver is used to solve the discrete RANS equations when the turbulent pulsation Mach number in the channel is low. This pressure-based

solver is developed by the PISO algorithm. The compressible reaction flow problem with a high Mach number can be solved correctly by the ddtFoam solver, which has less numerical dissipation at the point of discontinuity, so that it can be used for predicting the main parameters such as the velocity of propagation and the position of shock waves. The only drawback of the ddtFoam solver is that it does not work in very low Mach number flow. Thus, the PISO algorithm is implemented and can be utilized to start computations in stagnant flow, switching to the HLLC scheme once a combustion-induced flow has developed.

In the ddtFoam solver, instead of solving the transport equation for all chemical species reactions, only one transport equation was written and solved for the reaction progress variable c . The value of c was one for the burned mixture (the combustion products), and zero for unburned ones (reactants). In the ddtFoam solver, the auto-ignition delay time t_{ign} was computed using Arrhenius equations and based on the detailed reaction scheme introduced by O’Conaire et al. [54]. The composition of the mixture is defined using the mixture fraction (f_H), which is the hydrogen amount that would be present if the cell was completely unburned. Avoiding frequent re-computation of the local ignition delay time, a table of t_{ign} as a function of p , T , and (f_H) was produced using Cantera [55]. During numerical solutions, for each computational cell the local ignition delay time was achieved by searching the tabulated data [56].

The ddtFoam solver is designed for modeling accidental explosions in nuclear plants. This solver can be employed for detonation diffraction problems and various time-dependent extreme combustions. The capability of the ddtFoam solver to simulate the FA and DDT process on laboratory and industrial scales was shown in a variety of simulations [57,58]. In all simulations, the ddtFoam solver provides quick results with acceptable accuracy for analysis and design without the need for very fine grids. Imposing a Courant–Friedrichs–Lewy (CFL) number lower than 0.5 provided the good numerical stability of the ddtFoam solver. In this simulation, tolerance of 10^{-6} was set for all solution algorithms, the simulation time step was adaptive according to CFL number 0.3, and the value set for the size of the time step was 2×10^{-5} , which was the initial time step size.

2.6. Mesh Sensitivity Analysis and Boundary Conditions

Many combustion problems in a cylinder are axisymmetric, whereas CFD codes rarely include axisymmetric capabilities or cylindrical coordinates. In such cases, to accelerate the computation, a wedge of a small angle ($<5^\circ$) instead of the cylinder is usually selected. For axisymmetric problems, physical quantities such as chemical species concentrations, heat flux, temperature, and radiative intensity are different axially and radially only, so they are two-dimensional. Consequently, for many of these applications, the transport equations are solved on a thin wedge domain to lessen the computational effort. In the current simulation, in accordance with the cylindrical symmetry of the domain, there was an axis-symmetry geometry, so there was no need to mesh the whole pipe, but only a wedge of it, with an angle of 4 degrees. As $\partial/\partial\theta = 0$ for the whole domain, similar outcomes for 2D and 3D simulations were seen, while the number of elements in the mesh were less. A schematic of the wedge-type computational domain is shown in Figure 2.

In the current ENACCEF facility simulation, a uniform structured grid is used. To examine the mesh independency, four different computational meshes with cell sizes of 1 mm, 2 mm, 3 mm and 4 mm are generated. Due to the simplicity of the domain, OpenFOAM mesh generator blockMesh was utilized to produce the block-structured grid. Halouane et al. [39] simulated the ENACCEF facility in 2D and 3D forms. Both calculations gave the same results and effectively predicted pressure evolution and flame propagation.

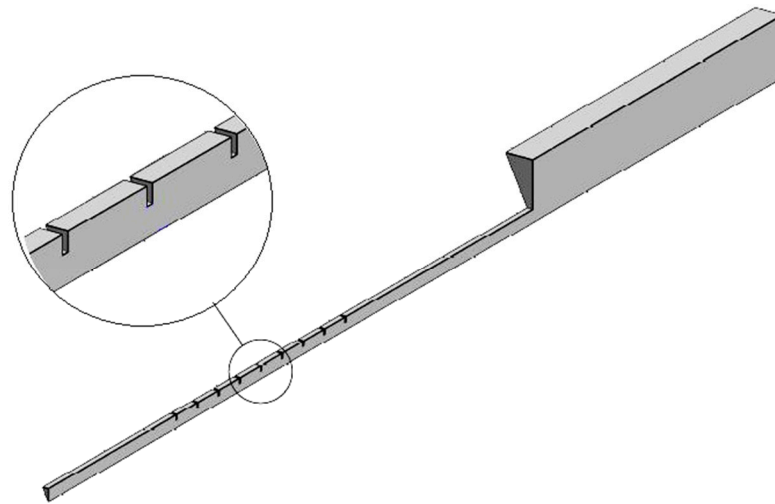


Figure 2. The schematic of the wedge-type computational domain.

Figure 3 depicts the flame front position with respect to time in the H_2 -air mixture with 13% hydrogen concentration and $BR = 0.63$. The flame front position is explained as the maximum vertical distance between the flame tip and the ignition point. This figure shows the mesh sensitivity analysis for the flame front position. In Figure 3, the slope of the flame front position changed near the first obstacle, about 0.6 m from the ignition point, and the slope further increased, which demonstrates that the obstacles offered a further increase in the velocity of the flame. The flame accelerated toward the dome and reached the end of it at about $t = 0.9$ s.

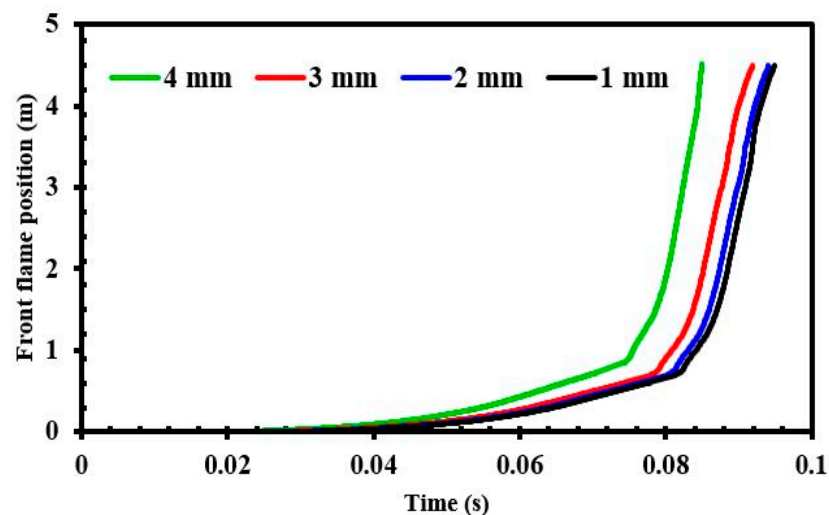


Figure 3. Mesh sensitivity analysis of H_2 -air mixture with a 13% hydrogen concentration for different computational grids.

Figure 4 indicates the relationship between the flame velocity and the elevation from the ignition point for the H_2 -air mixture with 30% hydrogen concentration and $BR = 0.63$. The speed of the flame was derived from the flame tip position. This figure shows the mesh sensitivity analysis for the flame velocity. In Figure 4, when $x < 1$ m, the velocity of the flame propagation showed an alternative “deceleration–acceleration” and an escalating trend of oscillation owing to the interaction between the flame, the obstacles, and the compression wave. At $x = 1$ m, an unexpected jump in flame speed was noticed, which is defined as the DDT. The maximum value of flame velocity was approximately 2500 m/s. Then, crossing the obstacle, the flame velocity declined and eventually stabilized at almost 2100 m/s.

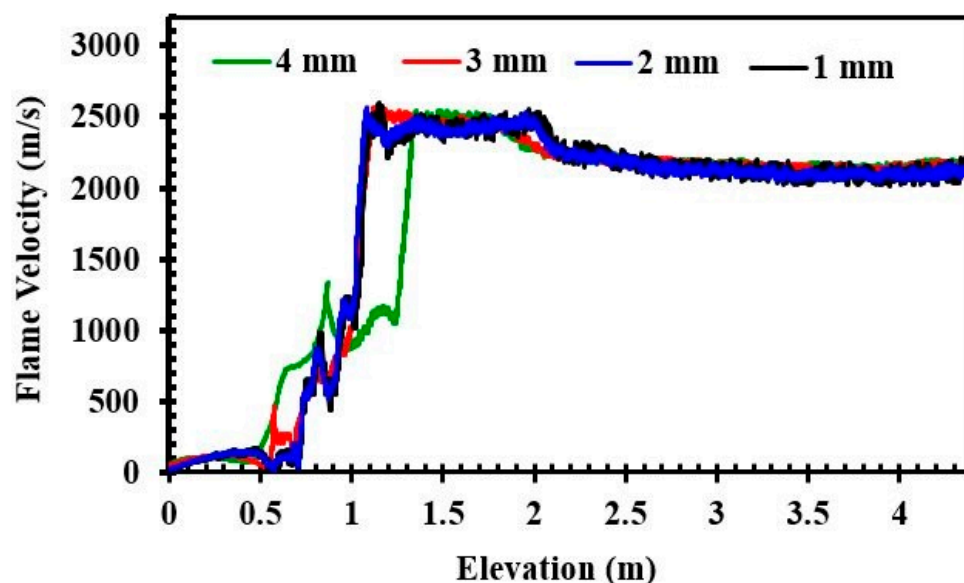


Figure 4. Mesh sensitivity analysis of H₂–air mixture with 30% hydrogen concentration for different computational grids.

For grid independence, cell sizes of 1 to 4 mm were examined for the flame tip position with respect to time in the H₂–air mixture with the hydrogen concentration of 13% (Figure 3), and flame velocity with respect to the elevation from the ignition point for the mixture with 30% hydrogen concentration (Figure 4). The results of the mesh independency study indicated that there was no considerable difference between grid sizes 1 mm (821,988 cells) and 2 mm (205,497 cells). Studying the results, it was found that reducing the computational grid size to less than 2 mm did not affect the accuracy of the solution or the DDT location. A 2-mm grid size was utilized by Ettner et al. [43]. Their simulations indicated that for the 2-mm cell size, the ddtFoam solver provides acceptable results compared to the experimental results [43,59]. Furthermore, Karanem et al. [44] and Shamsadin Saeid et al. [24,60] used an under-resolved grid size for deflagration to detonation simulations. A 2-mm grid size was applied in the current simulation, as under-resolved grids prepare computational scalability for greater geometries and allow flame acceleration and DDT studies in a time-limited manner. This is in line with the current work purpose to evolve the CFD flame acceleration and DDT modeling with the aim of obtaining scalability in greater areas.

The detonation propagation direction is from the bottom of the channel to the top. The upper and lower boundaries of the channel are considered as walls, where both velocity components on these boundaries are zero, and the fluid flow cannot leave or enter these boundaries. To make the present boundary condition closer to reality, no-slip boundary conditions were assumed for the wall boundaries of the chamber. The wall boundaries were considered adiabatic.

One of the most important parameters in simulating the acceleration of flame and DDT is applying the initial conditions in the numerical code. To observe the acceleration of flame and DDT, a fairly weak initiation is required at the beginning of the channel. After a weak initial flame is formed at the beginning of the channel, it propagates along the channel and increases the pressure and speed of the fluid flow. Subsequently, the acceleration steps provide the conditions required for the onset of detonation, whereby the transfer occurs. In the present simulation, the initial conditions were defined to initiate the problem solution with a weak flame with a radius of 10 mm at a distance of 0.138 m from the beginning of the channel. The mixture was assumed to be at rest, and the initial velocity was set to 0 m/s in the domain. Moreover, it was considered initially in the quiescent state and initialized with the experimental values of temperature and pressure. The initial conditions comprised a stationary mixture with a pressure of 1 atmosphere and a temperature of 296 Kelvin.

3. Results and Discussion

To validate the current numerical results, Figure 5a compares the experimental results of Bentaib et al. [17] and the numerical results of Halouane et al. [39] with the present numerical results. In this figure, the flame velocity and elevation from the ignition point are shown in the H₂–air mixture with 13% hydrogen concentration and BR = 0.63. According to the analysis of the experimental results, flame propagation in this chamber was divided into four parts: (1) the quasi-laminar flame (before reaching the obstructed part of the tube), (2) the accelerating flame (in the obstructed part of the tube), (3) the deceleration flame, (4) the flame jet occurring in the dome.

Based on the results presented in Figure 5a, there is a suitable agreement between the experimental and numerical results, and, therefore, the current solver could reproduce properties such as laminar and turbulent flame velocities for the hydrogen–air mixture. The current solver accurately captured important characteristics of the flow, contact discontinuity, rarefaction wave, and shock discontinuity, demonstrating that this solver can provide accurate shock capturing, and its results are confirmed. As seen, while the flame propagated in the obstructive tube, the flame velocity increased. The flame–turbulence interaction and surface area enhancement of the flame were found to be the reasons for flame velocity augmentation, which conclusively elevated the effective burning rate. Flame acceleration in the obstructive channel indicates the deflagration phase. The flame velocity reached its peak after the jet-like flame passed through the last obstacle. After that, it diminished due to the eradication of the turbulence flow created by the obstacles. In the absence of obstacles, flow turbulence was significantly reduced, and factors such as vortex–flame interactions and turbulence–flame, known to expand the flame surface area, could no longer be the major component of the flame acceleration phase. According to Figure 5a, for the concentration of 13%, the flame speed did not reach the sound speed of burned products, named choked flame. The emergence of a choked flame during acceleration of flame is vital for the DDT process in obstructed channels [61]. Thus, the transition to detonation did not occur inside the tube. By comparing the experiments and the simulations, it is clear that the simulations can represent the obtained processes experimentally. This simulation included various combustion modes such as slow and fast deflagration.

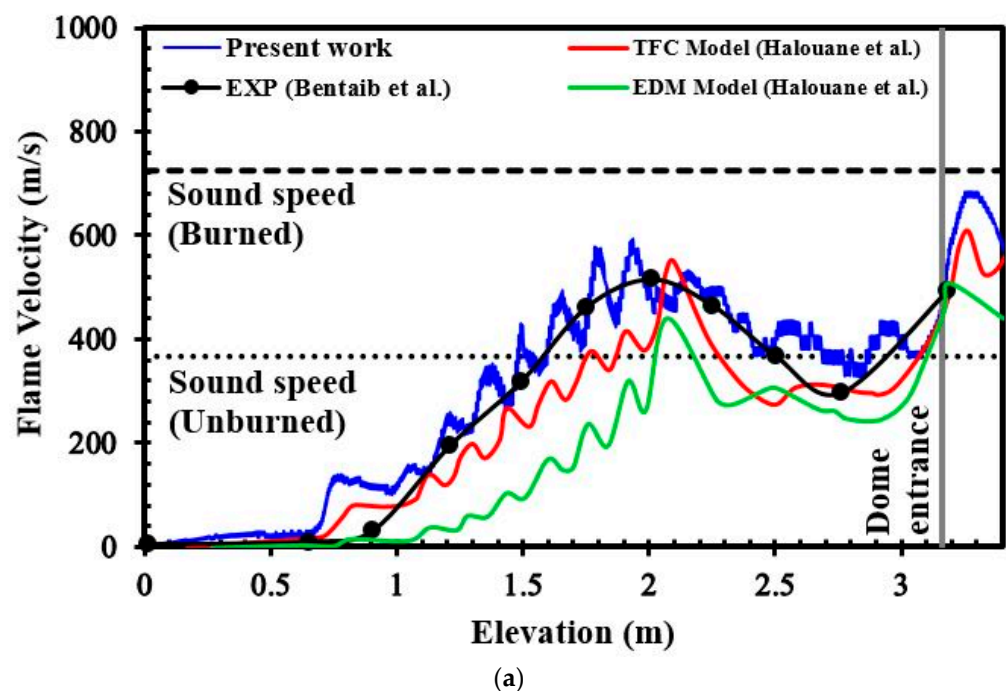


Figure 5. Cont.

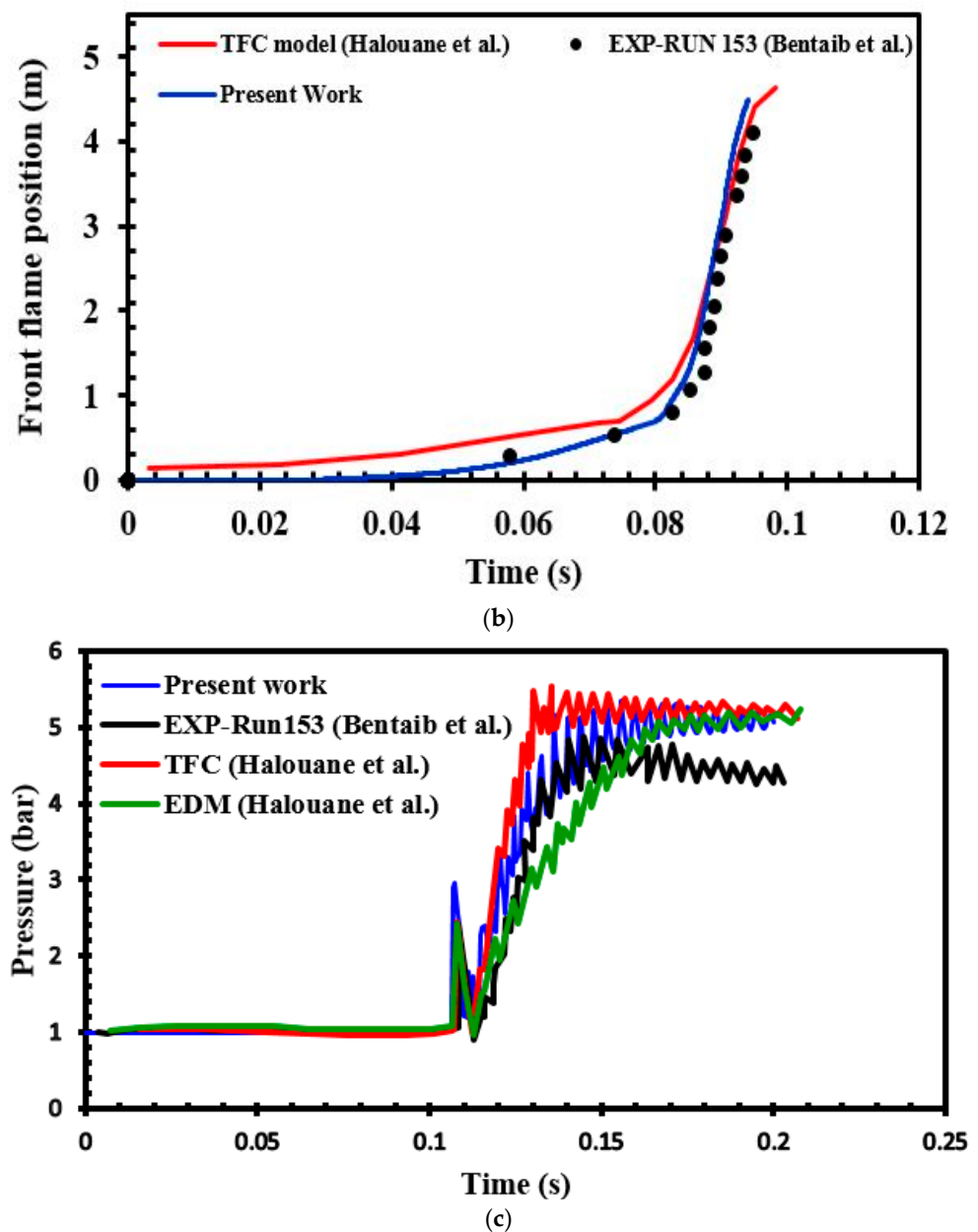


Figure 5. (a) The flame velocity in H_2 -air mixture with 13% hydrogen concentration, along with the experimental results of Bentaib et al. [17] and the numerical results of Halouane et al. [39]; (b) The front flame position in the mixture with 13% hydrogen concentration, along with the experimental results of Bentaib et al. [17] and the numerical results of Halouane et al. [39]; (c) The channel pressure history recorded at elevation 2.877 m in the mixture with 13% hydrogen concentration, along with the experimental results of Bentaib et al. [17] and the numerical results of Halouane et al. [39].

In Figure 5a, as can be observed, there was a small difference between the experimental and numerical results at the beginning of the channel. Based on examinations in lean mixtures by Hasselberg et al. [19], the Weller combustion model cannot properly simulate laminar flame. In lean mixtures, flame instabilities such as thermal-diffusive instabilities and Darrieus–Landau play a significant role in flame surface wrinkling during the modeling of slow laminar deflagration [62]. Furthermore, differences between the numerical and experimental diagrams may arise from the initial conditions considered for the spark. Therefore, the initial pressure wave generated in the experimental results may differ slightly from the initial pressure in numerical simulation. This spark influenced the flow field and then the flame speed.

Figure 5b,c indicate a comparison between the current simulation results, the experimental results of Bentaib et al. [17], and the numerical results of Halouane et al. [39] in the H₂–air mixture with 13% hydrogen concentration. Accordingly, the simulation outcomes are well matched with the data obtained experimentally. In Figure 5b, to make the comparison with the empirical data more straightforward, 20 ms was added to the time coordination of all the outputs obtained numerically. The key reason behind this time difference is in the ignition of the flame. In the experiment, the spark plug ignited only a very small volume of the mixture; therefore, there was a time lag before the starting time of flame propagation. Adding time to the numerical results was also undertaken by Kirkpatrick et al. [63]. The primary experiments showed that these differences were not essential points for the subsequent flame propagation. In Figure 5c, the pressure curve is adjusted by shifting time in order to allow a better comparison between simulation and experiments. Adding time to the numerical results in the pressure curves was also undertaken by Halouane et al. [39]. In this figure, the differences between the experimental and numerical results may arise from the heat losses as well as from radiation influences, which are not considered in this simulation.

To validate the current numerical results, Figure 6 compares the experimental results of Boeck et al. [64] and the numerical results of Karanam et al. [65] with the present numerical results. The numerical investigation of flame acceleration in a stratified mixture with 22.5% hydrogen concentration is conducted in the GraVent facility [64] with a length of 5.1 m and a rectangular cross section of height 60 mm and width 300 mm. The combustion chamber is completely smooth (blockage ratio BR = 0%). A transition of the flame regimes (i.e., slow flames, fast flames, and detonation) can be observed for the investigated mixture. At first, a fast flame is observed when the flame velocity exceeds the reactants' speed of sound and reaches the speed of sound of the products. After that, the flame velocity exceeds even the speed of sound of the products, and undergoes DDT further downstream.

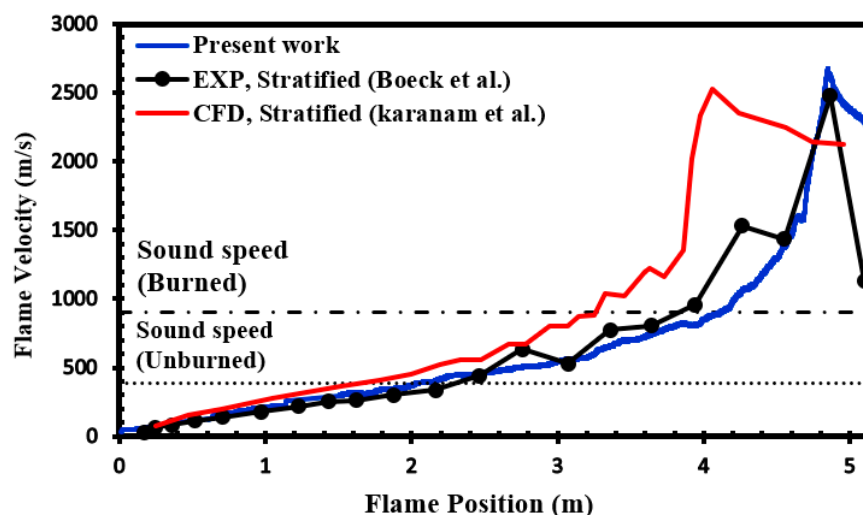


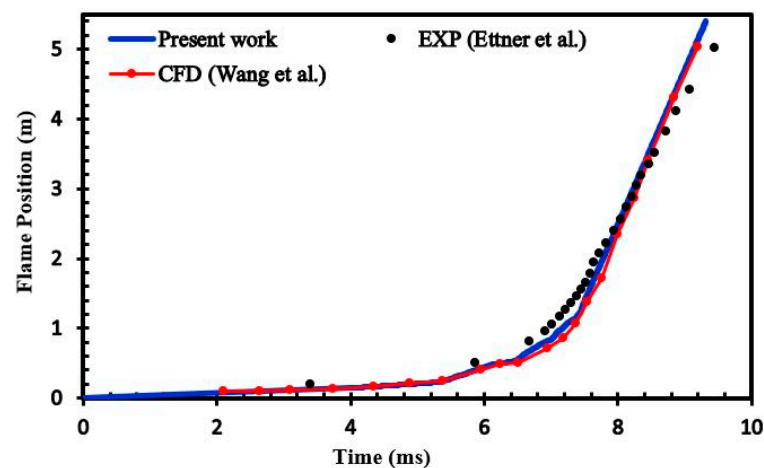
Figure 6. The flame velocity in the stratified H₂–air mixture with 22.5% hydrogen concentration, along with the experimental results of Boeck et al. [64] and the numerical results of Karanam et al. [65].

Figure 7a,b indicate a comparison between the current simulation results, the experimental results of Ettner et al. [43], and the numerical results of Wang et al. [66] in the inhomogeneous H₂–air mixture with 30% hydrogen concentration. The numerical investigation of flame acceleration is conducted in the GraVent facility [64] with a 5.4 m long tube and a rectangular cross section of height 60 mm and width 300 mm. The combustion chamber is partially equipped with turbulence-producing obstacles. In this configuration, the blockage ratio is chosen to be 60% and the distance between the obstacles is 300 mm. The first obstacle is at a distance of 0.25 m and the final obstacle is at a distance of 2.05 m from the ignition source. The remaining part of the tube is smooth. In Figure 7a, the simulation

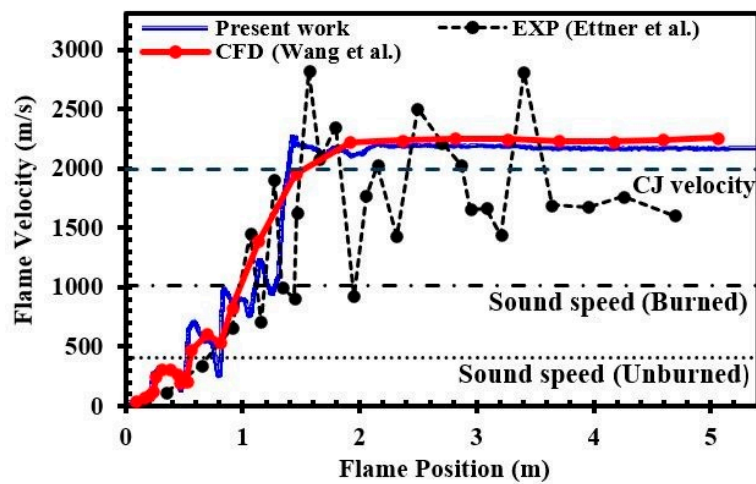
outcomes are well matched with the data obtained experimentally. In Figure 7b, compared to the simulation of Wang et al. [66], the present work better reproduces the deflagration to detonation location; however, both numerical results have significant differences with experimental results in predicting the steady detonation speed. Boeck et al. [64] have reported that the photodiode's measurements have an error for velocities above 1000 m/s in the GraVent facility. Figure 7c shows the predicted contours of temperature in the inhomogeneous H₂-air mixture with 30% hydrogen concentration. This figure reveals the field of view, including obstacles number three through five in the obstructed section of the tube during FA and DDT. At 7.0 ms the flame is about to interact with obstacle number three. At 7.1 ms, the flame is passing through the obstacles and a weak shock wave propagates ahead of the flame. At 7.4 ms, the strong shock wave has interacted with obstacle number four. Finally, formation of a strong Mach stem between obstacles number four and five causes the onset of detonation at 7.5 ms. This deflagration to detonation regime is close in similarity to the numerical results presented by Wang et al. [66].

Shamsadin Saeid et al. [24,60] also studied detonation using the ddtFoam solver in a rectangular channel with obstacles, and compared it with the experimental results of Ettner et al. [43] and Boeck et al. [67]. They showed that the solver has acceptable potential to study DDT. It should be noted that this is the first time that detonation has been studied in the ENACCEF facility. Figure 8 shows the flame speed for the H₂-air mixture with 20% hydrogen concentration and a blockage ratio of 0.63. As can be observed, the flame velocity fluctuates in the obstructed part of the tube due to the flame transporting through the obstacles. The flame speed rises while crossing the obstacle owing to the reduction in tube cross-section and increase in turbulence level. Then, crossing the obstacle, the flow decreases because of the abrupt flame expansion in the transverse direction and the rise in the cross-sectional area of the flow. Intense interactions between the propagating flame and the turbulent flow led the flame velocity to reach the sound speed of the unburned products and to transition from a slow to a fast deflagration and, eventually, to the choked flame. In this situation, owing to the interaction between the flame and the shock waves, the flame accelerated. Under these conditions, an unexpected jump in the velocity of the flame was seen, which is defined as DDT. Subsequently, the created detonation moved along the acceleration tube and entered the dome. Upon entering the dome, the detonation weakened, and local detonation damping was observed. This is associated with the effects of expansion waves and increased curvature. Furthermore, it was found that there was no total damping on detonation and, hence, the detonation was successfully released in a larger diameter tube at CJ speed.

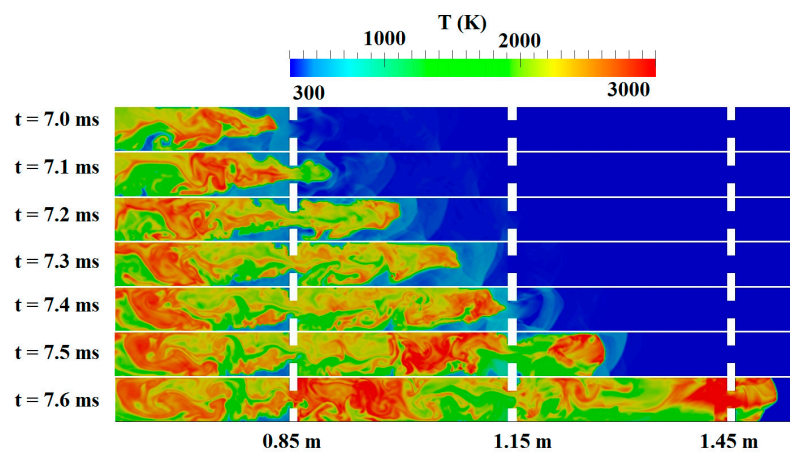
Figure 9 depicts the temperature and pressure contours in the dome area of the ENACCEF facility. In these contours, the detonation diffraction was investigated in an H₂-air mixture with 20% hydrogen concentration. At the dome entrance, expansion waves weakened the detonation. The area close to the bottom of the dome has the largest dilation gradient, which leads to the increase of spacing between detonation triple points and the attenuation of the detonation wave. Consequently, decoupling happens at the detonation wave, and the unburned zone is created at $t = 43.45$ ms. At this time, the motion of staggered triple points leads to local initiation on the center detonation front, therefore creating new transverse waves. Simultaneously, the center detonation wave ignites the combustible mixture in the unburned zone. The formation of the transverse detonation waves causes the extension of the center detonation wave in return. After that, the transverse detonation waves reach the bottom of the dome, and the re-initiation for the whole semi-circular detonation front is observed at $t = 43.50$ ms. In this case, the observed re-initiation of the diffracted detonation wave scenario is close in similarity to the numerical results proposed by Yuan et al. [27] through the straight channel. Then, the propagation process was conducted by reflected waves from the side wall of the dome behind the detonation front, as shown at $t = 43.60$ ms. The reflected waves from the tube walls collided at about $x = 3.5$ m in the central region of the dome and formed an area with very high temperature and pressure at $t = 43.85$ ms. This area makes the reinforcement and re-initiation of detonation.



(a)



(b)



(c)

Figure 7. (a) The flame-tip position at different times in the inhomogeneous H_2 -air mixture with 30% hydrogen concentration, along with the experimental results of Ettner et al. [43] and the numerical results of Wang et al. [66]. (b) The flame velocity in the inhomogeneous H_2 -air mixture with 30% hydrogen concentration, along with the experimental results of Ettner et al. [43] and the numerical results of Wang et al. [66]. (c) The predicted contours of temperature during FA and DDT in the inhomogeneous H_2 -air mixture with 30% hydrogen concentration.

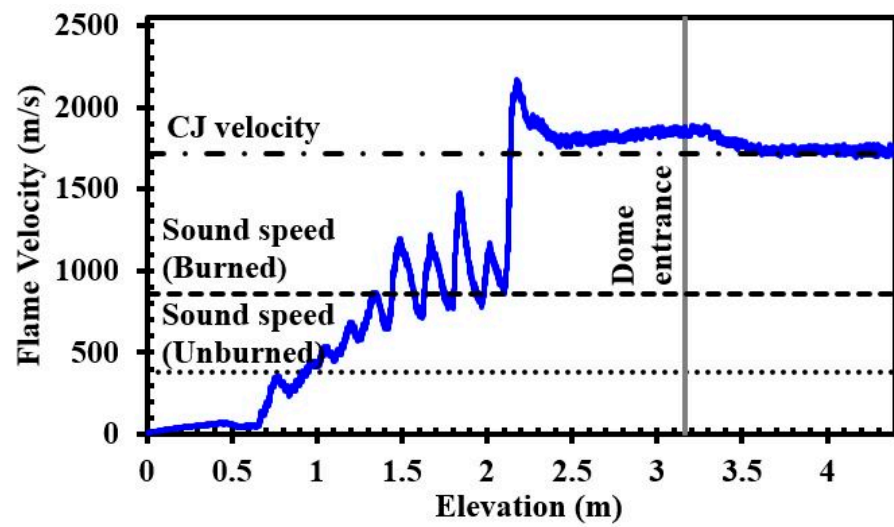


Figure 8. Flame velocity in H₂-air mixture with 20% hydrogen concentration.

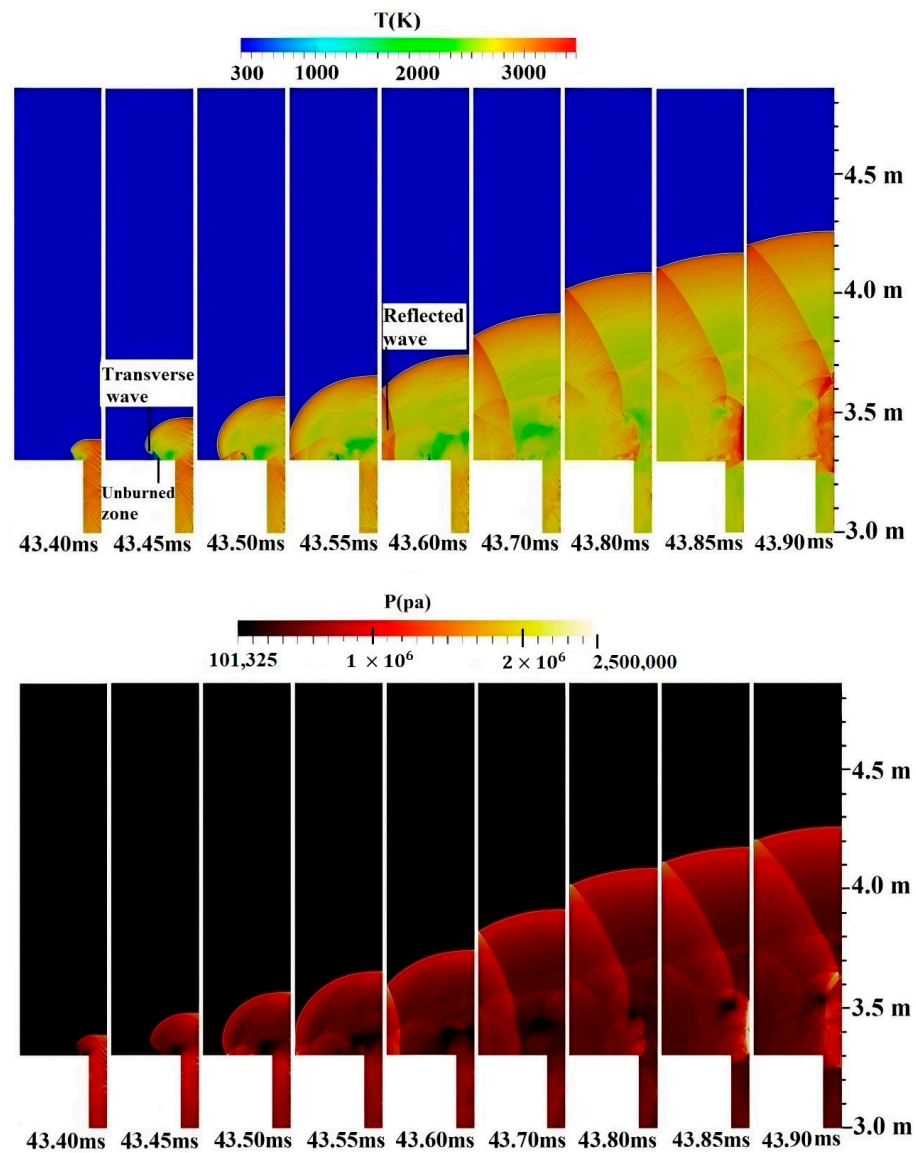


Figure 9. Temperature and pressure contours for the propagation of the flame in H₂-air mixture with 20% hydrogen concentration.

As shown in Figure 10, at one point in time, the speed of flame passed the sound speed of the burned products, and the flame entered the choked mode. At this point, an abrupt jump took place, and detonation initiation occurred. The created detonation was over-driven in the initial moments, and the detonation propagation velocity in the obstructed channel was about 250 m/s faster than in the unobstructed one. The presence of obstacles in the tube made the velocity of detonation propagation larger in this area. Then, the formed detonation wave reached its stable velocity (approximately 2100 m/s) and propagated to the end of the vertical vessel at the same velocity. When the hydrogen concentration grows to about 30%, the DDT time and location in the channel lessen. As seen, the concentration of 30% resulted in the fastest time for the occurrence of DDT. Based on the results proposed by Zheng et al. [32], four detonation initiation mechanisms can be observed in the main chamber: direct initiation, slow and fast deflagration to detonation transition initiation, and local explosion initiation. In the results presented in Figure 10, the direct initiation mechanism was observed for detonation diffraction, which is akin to the results obtained by Zheng et al. [32].

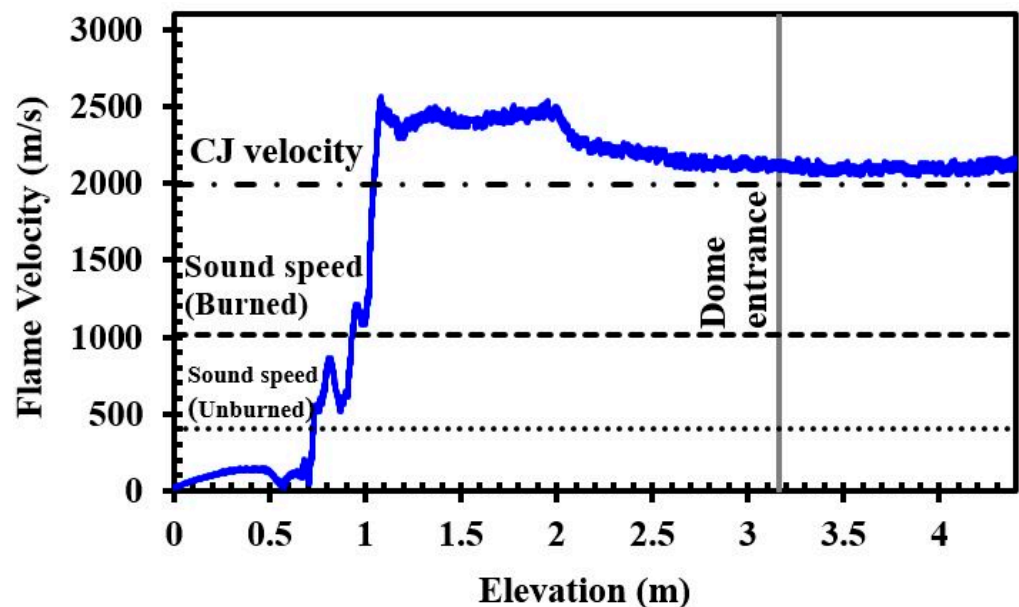


Figure 10. Flame-tip velocity in H_2 -air mixture with 30% hydrogen concentration.

Shown in Figure 11 are the temperature and pressure contours in the area around obstacles one to three. The occurrence of DDT in the H_2 -air mixture was investigated with 30% hydrogen concentration and $BR=0.63$ in these contours. At $t = 30.360$ ms, a hot spot or an explosion center appeared in the pressure and temperature contour after transporting the flame through obstacle number two. Then, this explosion center led to a local explosion, and the transition to detonation. It spread quickly and merged with the precursor shock. The detonation wave generated was overdriven. In these contours, Mach stem did not form; however, deflagration to detonation occurred near the flame front at the middle of the tube. This detonation regime is close in similarity to the results presented by Shamsadin Saeid et al. [24,60] and Gamezo et al. [68]. They examined DDT in a stoichiometric H_2 -air mixture. In their numerical simulations, the significance of Mach stem formation and its reflection from obstacles, and hence detonation wave formation, has been described. In some of their simulations, Mach stem formation was not observed. However, DDT occurred.

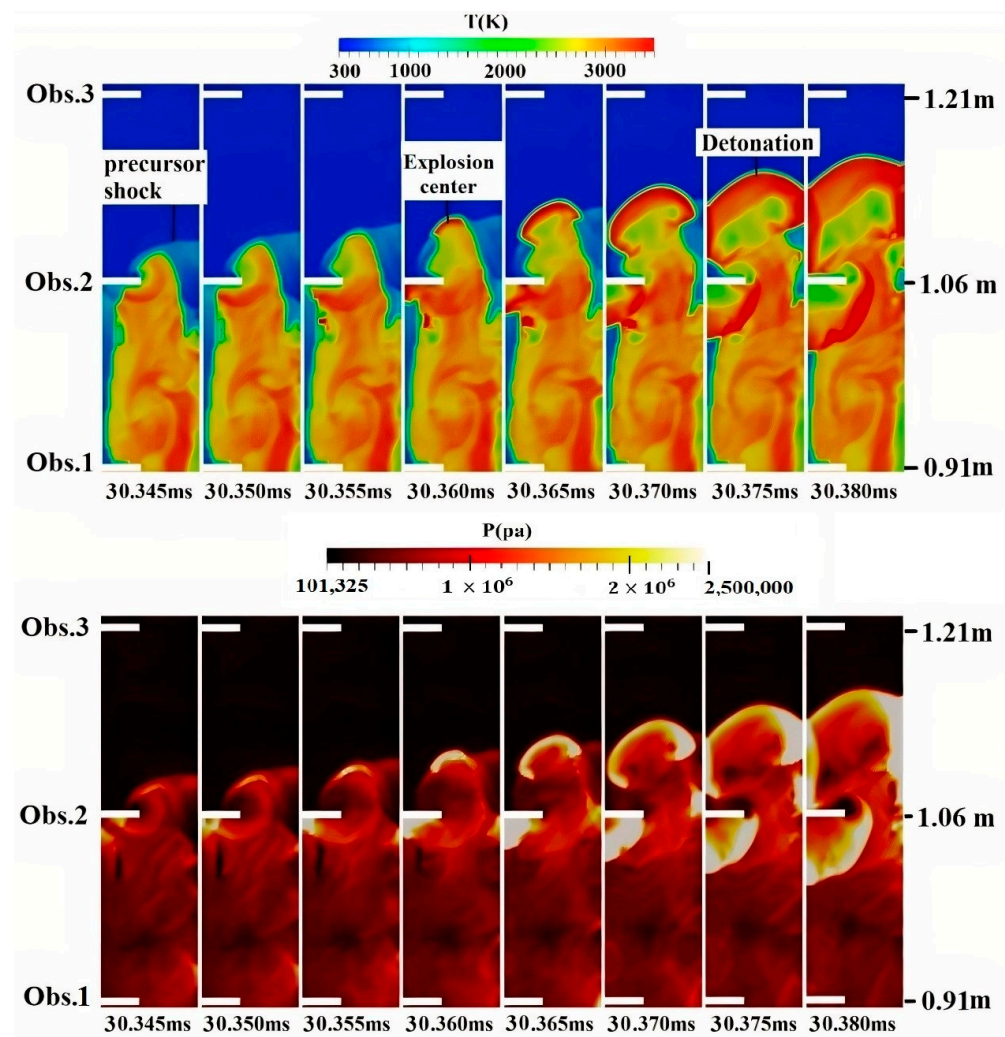


Figure 11. Temperature and pressure contours for the propagation of flame in H_2 –air mixture with 30% hydrogen concentration.

When the transition modes represent the direct detonation initiation at the inlet of the dome, it is described as the ideal detonation initiation for the dome using the acceleration tube. In this case, the propagation behavior is the supercritical condition discussed earlier. When the detonation wave propagated from the acceleration tube to the dome, it first experienced diffraction and later re-initiated, after numerous reflections, and returned to a self-sustaining propagation behavior. Consequently, detonation continued propagating along the centerline and encountered no failure. The concentration of the mixture is essential for the successful detonation re-initiation. Hence, the detonation re-initiation simulations were performed in different concentrations. Figure 12 shows the temperature and pressure contours in the ENACCEF facility in the H_2 –air mixture with 30% hydrogen concentration. As observed, the planar detonation wave created in the acceleration tube transitioned into a mushroom-like shape after entering the dome and causing re-initiation at the dome; therefore, it was named direct initiation. According to Figure 12, the spherical detonation wave was created at $t = 31.40$ ms, and it was expanded from the dome centerline to the surrounding area. As the detonation moved further, the transverse waves hit the dome wall and were reflected at $t = 31.50$ ms. The transverse waves reflected from the tube wall collided in the central region of the dome and formed an area with very high temperature and pressure at $t = 31.75$ ms. This area makes the reinforcement and re-initiation of detonation. The contrast is between the detonation attenuation by expansion waves and reinforcement of detonation owing to the reflection of the transverse waves and

the increase in the reaction rate. Unlike the subcritical regime, the disturbance propagating from the expansion boundary does not suppress the transmission of the incident detonation wave after the diffraction process. For a sufficiently supercritical detonation, while some separation of the reaction zone and the shock is still observed near the expansion boundary, the detonation propagates successfully after transitioning from a planar to a spherical wave. Figure 11 depicts the results for a supercritical detonation diffraction. The transversely propagating detonations are clearly visible. As shown in the results, any separation of the reaction zone and the shock near the expansion boundary is quickly overcome, and the detonation wave successfully transitioned into the dome without any signs of failure. This detonation diffraction can be classified into the supercritical regime. This supercritical detonation is close in similarity to the numerical results of Sinibaldi et al. [69] in a stoichiometric ethylene–oxygen mixture, and numerical and experimental results proposed by Peswani et al. [70].

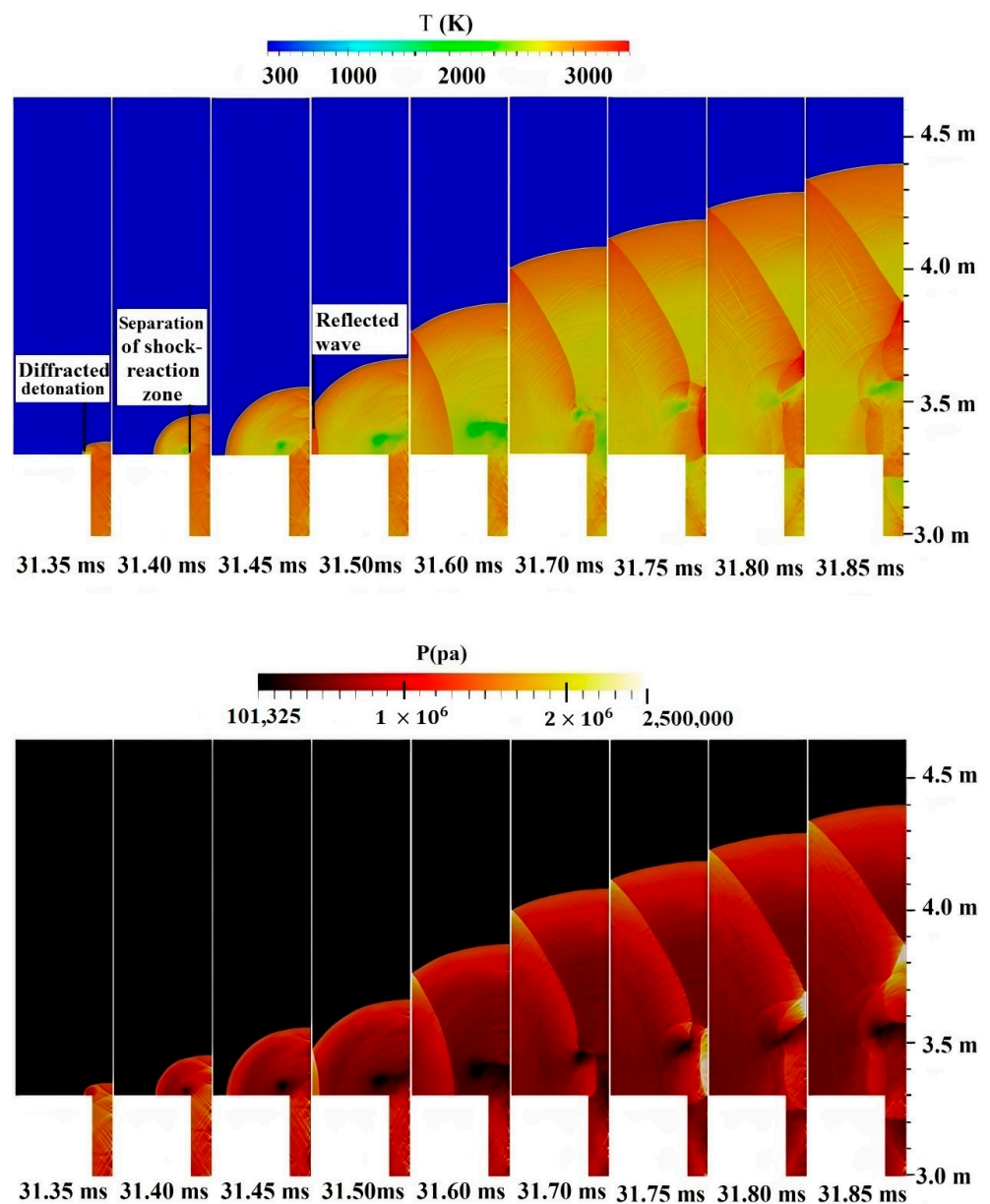


Figure 12. The temperature and pressure contours for the propagation of the flame in the H₂–air mixture with 30% hydrogen concentration.

To sum up, the diffraction of the detonation wave via the dome part weakened the intensity of the leading shock, decoupled the detonation wave, and declined the rate of chemical reaction behind the leading shock. Then, multiple reflections appeared in the tube, and the detonation wave was re-initiated by the interaction of Mach shock, reflected wave, and transverse detonation wave.

4. Conclusions

In this research, the phenomenon of gas detonation diffraction was investigated, and the behavior of the detonation during diffraction and changes in the detonation surface area were examined. The OpenFOAM platform was applied to examine the impact of hydrogen concentration on FA and DDT in a mixture with different hydrogen concentrations in a vertical vessel. The results showed that mixture concentration can be an influential factor in the acceleration of flame and the location of detonation initiation.

Below are the main conclusions of this study:

- In the current numerical simulation, the PISO algorithm and ddtFoam solver were combined. The proposed simulation method is suitable for laminar flow with low Mach number, compressible reaction flow with high Mach number, and turbulent flow. It can predict the FA and DDT in detonation engines and hydrogen combustion. This method can also calculate properties of the flame propagation and pressure transients with a relatively coarse mesh, thus making it possible to balance computational time and computational accuracy.
- In an H₂–air mixture with 13% hydrogen concentration, flame acceleration in the obstructive channel indicates the deflagration phase. The major mechanism of combustion propagation is of a flame front that moves forward through the gas mixture. In technical terms the reaction zone progresses through the medium by processes of diffusion of heat and mass. When the flame propagates in the obstructed part of the tube, the speed of flame increases owing to expansion in the flame surface area and the flame–turbulence interaction. These two factors increase the effective burning rate. Moreover, the weak flame acceleration showed the unstable flame phase. In this mode, flame velocity did not reach the sound speed in the combustion products and DDT did not occur inside the tube.
- For H₂–air mixture with 20% hydrogen concentration, the turbulence increased the burning rate by increasing the rate of heat and mass transfer and the area of the flame front. As a result, propagation of the flame front accelerated, and the detonation initiation occurred in the acceleration tube. The results revealed that the expansion waves weakened the detonation in the region where the channel width changed, and the weakened detonation became stable once it progressed further. The governing flow regime of the detonation diffraction was supercritical, after which the detonation was successfully propagated.
- For the mixture with a hydrogen concentration of 30%, heat and mass transfer from the flame were responsible for emerging the explosion center that caused the detonation. The condition of the mixture in the neighborhood of the explosion center must also be conducive to the amplification of the shock wave from the explosion center in order to result in the generation of the overdriven detonation wave. In an H₂–air mixture with 30% hydrogen concentration, the governing detonation diffraction mechanism was direct initiation. The detonation wave generated in the acceleration tube area moved to the dome area, and the detonation was successfully and steadily propagated in the diffraction region. With the increase in the concentration of the hydrogen–air mixture up to 30%, the time and location of the detonation initiation in the acceleration tube diminished.

The next step to be undertaken as a future direction is to expand such numerical studies into a 3D state and implement them using industry-scale geometries. Furthermore, a critical future path is to investigate the sub-scale processes such as induction distance, interaction of shock boundary layer, and instabilities resulting from the interaction between

expanding flame and shock. This can be achieved by using models with higher resolution such as LES in industry-scale geometries.

Author Contributions: Conceptualization, M.H.S.S.; methodology, M.H.S.S. and M.G.; software, M.H.S.S.; validation, M.H.S.S. and M.G.; formal analysis, M.H.S.S.; investigation, M.H.S.S.; resources, M.G.; data curation, M.G.; writing—original draft preparation, M.H.S.S.; writing—review and editing, M.H.S.S. and M.G.; supervision, M.G. All authors have read and agreed to the published version of the manuscript.

Funding: This research received no external funding.

Data Availability Statement: The data presented in this study are available on request from the corresponding author.

Conflicts of Interest: The authors declare no conflict of interest.

Nomenclature

a	Thermal diffusivity (m ² /s)
BR	Blockage ratio
c	Reaction progress variable
CFL	Courant–Friedrichs–Lewy
CJ	Chapman–Jouget
D	Molecular diffusion coefficient (m ² /s)
DDT	Deflagration-to-detonation transition
e_t	Total internal energy (J/kg)
FA	Flame acceleration
f_H	Hydrogen mixture fraction
g	Body force (m ² /s)
k	Turbulent kinetic energy (J/kg)
p	Pressure (Pa)
PDE	Pulse detonation engine
PISO	Pressure Implicit with Splitting of Operator
R	Specific gas constant
SST	Shear Stress Transport
S_l	laminar burning speed
S_T	turbulent burning speed
t	Time (s)
t_{ign}	Auto-ignition delay time (s)
u	Velocity (m/s)
Greek Symbols	
ζ	flame wrinkling factor
ρ	Density (kg/m ³)
δ_{ij}	Kronecker delta
μ	Dynamic viscosity (kg/m s)
$\omega_{c,def}$	Deflagrative source term for reaction progress variable (kg/m ³ s)
$\omega_{c,ign}$	Ignition source term for reaction progress variable (kg/m ³ s)

References

1. Wu, Y. Assessment of the impact of jet flame hazard from hydrogen cars in road tunnels. *Eng. Environ. Sci.* **2008**, *16*, 246–254. [[CrossRef](#)]
2. Pintgen, F.; Shepherd, J. Detonation diffraction in gases. *Combust. Flame* **2009**, *156*, 665–677. [[CrossRef](#)]
3. Li, L.; Li, J.-M.; Teo, C.J.; Chang, P.-H.; Nguyen, V.B.; Khoo, B.C. On the Investigation of Detonation Re-initiation Mechanisms and the Influences of the Geometry Confinements and Mixture Properties. In *Detonation Control for Propulsion*; Springer: Berlin/Heidelberg, Germany, 2017; pp. 199–235. [[CrossRef](#)]
4. Polley, N.L.; Egbert, M.Q.; Petersen, E.L. Methods of re-initiation and critical conditions for a planar detonation transforming to a cylindrical detonation within a confined volume. *Combust. Flame* **2012**, *160*, 212–221. [[CrossRef](#)]
5. Radulescu, M.; Sharpe, G.; Lee, J.; Kiyanda, C.; Higgins, A.; Hanson, R. The ignition mechanism in irregular structure gaseous detonations. *Proc. Combust. Inst.* **2005**, *30*, 1859–1867. [[CrossRef](#)]

6. Knystautas, R.; Lee, J.; Guirao, C. The critical tube diameter for detonation failure in hydrocarbon-air mixtures. *Combust. Flame* **1982**, *48*, 63–83. [[CrossRef](#)]
7. Moen, I.; Murray, S.; Bjerketvedt, D.; Rinnan, A.; Knystautas, R.; Lee, J. Diffraction of detonation from tubes into a large fuel-air explosive cloud. *Symp. (Int.) Combust.* **1982**, *19*, 635–644. [[CrossRef](#)]
8. Murray, S.; Lee, J. On the transformation of planar detonation to cylindrical detonation. *Combust. Flame* **1983**, *52*, 269–289. [[CrossRef](#)]
9. Teodorczyk, A.; Lee, J.; Knystautas, R. The structure of fast turbulent flames in very rough, obstacle-filled channels. *Symp. (Int.) Combust.* **1991**, *23*, 735–741. [[CrossRef](#)]
10. Dupre, G.; Peraldi, O.; Lee, J.H.; Knystautas, R. Propagation of detonation waves in an acoustic absorbing walled tube. *AIAA Program Astronaut Aeronaut* **1988**, *114*, 248–263. [[CrossRef](#)]
11. Lee, J.H.S. Initiation of Gaseous Detonation. *Annu. Rev. Phys. Chem.* **1977**, *28*, 75–104. [[CrossRef](#)]
12. Li, Y.Z. Study of fire and explosion hazards of alternative fuel vehicles in tunnels. *Fire Saf. J.* **2019**, *110*, 102871. [[CrossRef](#)]
13. Gamezo, V.N.; Ogawa, T.; Oran, E.S. Numerical simulations of flame propagation and DDT in obstructed channels filled with hydrogen–air mixture. *Proc. Combust. Inst.* **2007**, *31*, 2463–2471. [[CrossRef](#)]
14. Ciccarelli, G.; Dorofeev, S. Flame acceleration and transition to detonation in ducts. *Prog. Energy Combust. Sci.* **2008**, *34*, 499–550. [[CrossRef](#)]
15. Kessler, D.; Gamezo, V.; Oran, E. Simulations of flame acceleration and deflagration-to-detonation transitions in methane–air systems. *Combust. Flame* **2010**, *157*, 2063–2077. [[CrossRef](#)]
16. Na'Inna, A.M.; Phylaktou, H.; Andrews, G.E. Effects of Obstacle Separation Distance on Gas Explosions: The Influence of Obstacle Blockage Ratio. *Procedia Eng.* **2014**, *84*, 306–319. [[CrossRef](#)]
17. Bentaib, A.; Bleyer, A.; Meynet, N.; Chaumeix, N.; Schramm, B.; Höhne, M.; Kostka, P.; Movahed, M.; Worapittayaporn, S.; Brähler, T.; et al. SARNET hydrogen deflagration benchmarks: Main outcomes and conclusions. *Ann. Nucl. Energy* **2014**, *74*, 143–152. [[CrossRef](#)]
18. Emami, S.; Mazaheri, K.; Shamooni, A.; Mahmoudi, Y. LES of flame acceleration and DDT in hydrogen–air mixture using artificially thickened flame approach and detailed chemical kinetics. *Int. J. Hydrogen Energy* **2015**, *40*, 7395–7408. [[CrossRef](#)]
19. Hasslberger, J.; Boeck, L.R.; Sattelmayer, T. Numerical simulation of deflagration-to-detonation transition in large confined volumes. *J. Loss Prev. Process Ind.* **2015**, *36*, 371–379. [[CrossRef](#)]
20. Ciccarelli, G.; Cross, M. On the propagation mechanism of a detonation wave in a round tube with orifice plates. *Shock Waves* **2016**, *26*, 587–597. [[CrossRef](#)]
21. Zhu, R.; Zhao, M.; Zhang, H. Numerical simulation of flame acceleration and deflagration-to-detonation transition in ammonia-hydrogen–oxygen mixtures. *Int. J. Hydrogen Energy* **2020**, *46*, 1273–1287. [[CrossRef](#)]
22. Ni, J.; Pan, J.; Zhu, Y. Effect of arc obstacles blockage ratio on detonation characteristics of hydrogen-air. *Acta Astronaut* **2020**, *170*, 188–197. [[CrossRef](#)]
23. Sun, X.; Lu, S. Effect of orifice plate on the transmission mechanism of a detonation wave in hydrogen-oxygen mixtures. *Int. J. Hydrogen Energy* **2020**, *45*, 12593–12603. [[CrossRef](#)]
24. Saeid, M.H.S.; Khadem, J.; Emami, S. Numerical investigation of the mechanism behind the deflagration to detonation transition in homogeneous and inhomogeneous mixtures of H₂-air in an obstructed channel. *Int. J. Hydrogen Energy* **2021**, *46*, 21657–21671. [[CrossRef](#)]
25. Liu, Y.; Yang, X.; Fu, Z.; Chen, P. Numerical simulation of flame acceleration and DDT (deflagration to detonation transition) in hydrogen-air mixtures with concentration gradients. *Energy Sources Part A Recover. Util. Environ. Eff.* **2021**, 1–17. [[CrossRef](#)]
26. Soleimanpour, R.; Nemati, H.; Zare, A. Comprehensive studies on suitable reaction mechanisms to predict the behavior of high speed reacting flows. *Chem. Eng. Commun.* **2021**, 1–12. [[CrossRef](#)]
27. Yuan, X.Q.; Mi, X.C.; Ng, H.D.; Zhou, J. A model for the trajectory of the transverse detonation resulting from re-initiation of a diffracted detonation. *Shock Waves* **2020**, *169*, 94–107. [[CrossRef](#)]
28. Shi, L.; Uy, K.C.K.; Wen, C.Y. The re-initiation mechanism of detonation diffraction in a weakly unstable gaseous mixture. *J. Fluid Mech.* **2020**, *895*, 1–35. [[CrossRef](#)]
29. Schultz, E. Detonation Diffraction Through an Abrupt Area Expansion. Ph.D. Thesis, California Institute of Technology, Pasadena, CA, USA, 2000. [[CrossRef](#)]
30. Papalexandris, M.; Thomas, J.; Jacobs, C.; Deledicque, V. Structural characteristics of detonation expansion from a small channel to a larger one. *Proc. Combust. Inst.* **2007**, *31*, 2407–2414. [[CrossRef](#)]
31. Sun, X.; Li, Q.; Xu, M.; Wang, L.; Guo, J.; Lu, S. Experimental study on the detonation propagation behaviors through a small-bore orifice plate in hydrogen-air mixtures. *Int. J. Hydrogen Energy* **2019**, *44*, 15523–15535. [[CrossRef](#)]
32. Zheng, J.; Lei, Q.; Zhao, X.; Fan, W. Experimental characterization of detonation initiation modes in a confined chamber flush-mounted with small-diameter ignition tubes. *Proc. Combust. Inst.* **2020**, *38*, 3741–3748. [[CrossRef](#)]
33. Lei, Q.; Zhao, X.; Zheng, J.; He, J.; Wang, K.; Fan, W. Role of overdriven state of ignition wave in pre-detonators on detonation transition modes in a flat chamber. *Aerosp. Sci. Technol.* **2021**, *115*, 106771. [[CrossRef](#)]
34. Li, Q.; Kellenberger, M.; Ciccarelli, G. Geometric influence on the propagation of the quasi-detonations in a stoichiometric H₂-O₂ mixture. *Fuel* **2020**, *269*, 117396. [[CrossRef](#)]

35. Schiavetti, M.; Carcassi, M. Experimental tests of inhomogeneous hydrogen deflagrations in the presence of obstacles. *Int. J. Hydrogen Energy* **2020**, *46*, 12455–12463. [CrossRef]
36. Wang, L.-Q.; Ma, H.-H.; Shen, Z.-W.; Pan, J. Detonation Re-initiation behind an Aluminum Foam Plate in Stoichiometric Methane-oxygen Mixture. *Combust. Sci. Technol.* **2021**, *194*, 2836–2846. [CrossRef]
37. Yin, Z.; Wang, Z.; Cao, X.; Zhen, Y.; Jiang, K.; Ma, S.; Gao, W. Effects of Obstacles on Deflagration-to-Detonation Transition in Linked Vessels. *Combust. Sci. Technol.* **2022**, *194*, 1265–1281. [CrossRef]
38. Sun, H.; Kawasaki, A.; Matsuoka, K.; Kasahara, J. A study on detonation-diffraction reflection point distances in H₂/O₂, C₂H₂/O₂, and C₂H₄/O₂ systems. *Proc. Combust. Inst.* **2020**, *38*, 3605–3613. [CrossRef]
39. Halouane, Y.; Dehbi, A. CFD simulations of premixed hydrogen combustion using the Eddy Dissipation and the Turbulent Flame Closure models. *Int. J. Hydrogen Energy* **2017**, *42*, 21990–22004. [CrossRef]
40. Kang, H.; Kim, J.; Hong, S.; Kim, S. Numerical Analysis for Hydrogen Flame Acceleration during a Severe Accident in the APR1400 Containment Using a Multi-Dimensional Hydrogen Analysis System. *Energies* **2020**, *13*, 6151. [CrossRef]
41. Cherbański, R.; Molga, E. CFD simulations of hydrogen deflagration in slow and fast combustion regime. *Combust. Theory Model.* **2020**, *24*, 589–605. [CrossRef]
42. Li, M.; Li, D.; Xu, Y.; Wen, X.; Liu, S. Effects of obstacle position and number on the overpressure of hydrogen combustion in a semi-confined compartment. *J. Nucl. Sci. Technol.* **2018**, *55*, 634–639. [CrossRef]
43. Ettner, F.; Vollmer, K.G.; Sattelmayer, T. Numerical Simulation of the Deflagration-to-Detonation Transition in Inhomogeneous Mixtures. *J. Combust.* **2014**, *2014*, 686347. [CrossRef]
44. Karanam, A.; Ganju, S.; Chattopadhyay, J. Timescale analysis, numerical simulation and validation of flame acceleration, and DDT in Hydrogen–Air mixtures. *Combust. Sci. Technol.* **2021**, *193*, 2217–2240. [CrossRef]
45. Liu, X.-Y.; Luan, M.-Y.; Chen, Y.-L.; Wang, J.-P. Flow-field analysis and pressure gain estimation of a rotating detonation engine with banded distribution of reactants. *Int. J. Hydrogen Energy* **2020**, *45*, 19976–19988. [CrossRef]
46. Olcucuoglu, B.; Saracoglu, B.H. A preliminary heat transfer analysis of pulse detonation engines. *Transp. Res. Procedia* **2018**, *29*, 279–288. [CrossRef]
47. Olcucuoglu, B.; Temel, O.; Tuncer, O.; Saracoglu, B.H. A Novel Open Source Conjugate Heat Transfer Solver for Detonation Engine Simulations. In Proceedings of the 2018 AIAA Aerospace Sciences Meeting, Kissimmee, FL, USA, 8–12 January 2018. [CrossRef]
48. Weller, H.; Tabor, G.; Gosman, A.; Fureby, C. Application of a flame-wrinkling les combustion model to a turbulent mixing layer. *Symp. (Int.) Combust.* **1998**, *27*, 899–907. [CrossRef]
49. Menter, F. Improved two-equation k-omega turbulence models for aerodynamic flows. *NASA Tech. Memo.* **1992**, *93*, 22809.
50. Peters, N. *Turbulent Combustion*; Cambridge University Press: New York, NY, USA, 2000.
51. Khodadadi Azadboni, R. Numerical Modelling of Inhomogeneous Liquefied Natural Gas (LNG) Vapor Cloud Explosions. Ph.D. Thesis, Department of Mechanical and Automotive Engineering, Kingston University, Kingston, UK, 2019.
52. Middha, P.; Hansen, O.R. Predicting deflagration to detonation transition in hydrogen explosions. *Process Saf. Prog.* **2007**, *27*, 192–204. [CrossRef]
53. Ettner, F.; Sattelmayer, T. ddtFoam 2014. Available online: <https://sourceforge.net/projects/ddtfoam> (accessed on 5 May 2014).
54. Conaire, M.; Curran, H.J.; Simmie, J.M.; Pitz, W.J.; Westbrook, C.K. A comprehensive modeling study of hydrogen oxidation. *Int. J. Chem. Kinet.* **2004**, *36*, 603–622. [CrossRef]
55. Goodwin, D.G.; Moffat, H.; Speth, R.L. Cantera: An Object-oriented Software Toolkit for Chemical Kinetics, Thermodynamics, and Transport Processes 2016. Available online: <http://code.google.com/p/cantera> (accessed on 26 January 2016).
56. Bassi, V.; Vohra, U.; Singh, R.; Jindal, T.K. Numerical Study of Deflagration to Detonation Transition Using Obstacle Combinations in OpenFOAM. In Proceedings of the 2020 IEEE Aerospace Conference, Big Sky, MT, USA, 7–14 March 2020; pp. 1–15. [CrossRef]
57. Wang, J.; Zhao, X.; Gao, L.; Wang, X.; Zhu, Y. Effect of solid obstacle distribution on flame acceleration and DDT in obstructed channels filled with hydrogen-air mixture. *Int. J. Hydrogen Energy* **2022**, *47*, 12759–12770. [CrossRef]
58. Rudy, W.; Teodorczyk, A. Numerical Simulations of DDT Limits in Hydrogen-Air Mixtures in Obstacle Laden Channel. *Energies* **2021**, *14*, 24. [CrossRef]
59. Ettner, F.; Sattelmayer, T. Effiziente numerische Simulation des Deflagrations-Detonations-Übergangs. Ph.D. Thesis, Technical University of Munich, Munich, Germany, 2013. (In German)
60. Saeid, M.H.S.; Khadem, J.; Emami, S.; Ghodrat, M. Effect of diffusion time on the mechanism of deflagration to detonation transition in an inhomogeneous mixture of hydrogen-air. *Int. J. Hydrogen Energy* **2022**, *47*, 23411–23426. [CrossRef]
61. Emami, S.; Mazaheri, K.; Shamooni, A.; Mahmoudi, Y. Numerical simulation of flame acceleration, and fast deflagrations using artificial thickening flame approach. In Proceedings of the 25th International Colloquium on the Dynamics of Explosions and Reactive Systems (ICDRS), Leeds, UK, 2–7 August 2015; University of Leeds: Leeds, UK, 2015.
62. Landau, L. On the Theory of Slow Combustion. In *Dynamics of Curved Fronts*; Academic Press: Cambridge, MA, USA, 1988; pp. 403–411. [CrossRef]
63. Kirkpatrick, M.P.; Armfield, S.W.; Masri, A.R.; Ibrahim, S.S. Large eddy simulation of a propagating turbulent premixed flame. *Flow Turbul. Combust.* **2003**, *70*, 1–19. [CrossRef]
64. Boeck, L.R.; Katzy, P.; Hasslberger, J.; Kink, A.; Sattelmayer, T. The GraVent DDT database. *Shock Waves* **2016**, *26*, 683–685. [CrossRef]

65. Karanam, A.; Sharma, P.K.; Ganju, S. Numerical simulation and validation of flame acceleration and DDT in hydrogen air mixtures. *Int. J. Hydrogen Energy* **2018**, *43*, 17492–17504. [[CrossRef](#)]
66. Wang, C.; Wen, J. Numerical simulation of flame acceleration and deflagration-to-detonation transition in hydrogen-air mixtures with concentration gradients. *Int. J. Hydrogen Energy* **2017**, *42*, 7657–7663. [[CrossRef](#)]
67. Boeck, L.R.; Hasslberger, J.; Ettner, F.; Sattelmayer, T. Investigation of Peak Pressures During Explosive Combustion of Inhomogeneous Hydrogen-Air Mixtures. In Proceedings of the Seventh International Seminar Fire and Explosion Hazards, Providence, RI, USA, 5–10 May 2013. [[CrossRef](#)]
68. Gamezo, V.N.; Ogawa, T.; Oran, E.S. Flame acceleration and DDT in channels with obstacles: Effect of obstacle spacing. *Combust. Flame* **2008**, *55*, 302–315. [[CrossRef](#)]
69. Sinibaldi, J.O.; Brophy, C.M. Initiator Detonation Diffraction Studies in Pulsed Detonation Engines. In Proceedings of the 37th Joint Propulsion Conference and Exhibit, Salt Lake City, UT, USA, 8–11 July 2001. [[CrossRef](#)]
70. Peswani, M.; Floring, G.; Maxwell, B. Simulating the critical regime following detonation diffraction in a weakly unstable mixture. In Proceedings of the Spring Technical Meeting of The Central States Section of the Combustion Institute, Detroit, MI, USA, 15–17 May 2022.